INTERFACE

Research

CrossMark
click for updates

Author for correspondence:
Kevin J. Painter
e-mail: k.painter@hw.ac.uk

THE ROYAL SOCIETY
PUBLISHING

Navigating the flow: individual and continuum models for homing in flowing environments

Kevin J. Painter[1] and Thomas Hillen[2]

[1]Department of Mathematics and Maxwell Institute for Mathematical Sciences, Heriot-Watt University, Edinburgh, UK
[2]Centre for Mathematical Biology, University of Alberta, Edmonton, Alberta, Canada

Navigation for aquatic and airborne species often takes place in the face of complicated flows, from persistent currents to highly unpredictable storms. Hydrodynamic models are capable of simulating flow dynamics and provide the impetus for much individual-based modelling, in which particle-sized individuals are immersed into a flowing medium. These models yield insights on the impact of currents on population distributions from fish eggs to large organisms, yet their computational demands and intractability reduce their capacity to generate the broader, less parameter-specific, insights allowed by traditional continuous approaches. In this paper, we formulate an individual-based model for navigation within a flowing field and apply scaling to derive its corresponding macroscopic and continuous model. We apply it to various movement classes, from drifters that simply go with the flow to navigators that respond to environmental orienteering cues. The utility of the model is demonstrated via its application to 'homing' problems and, in particular, the navigation of the marine green turtle *Chelonia mydas* to Ascension Island.

1. Introduction

More than a century ago, Charles Darwin [1] remarked on the astonishing voyages of adult green turtles, during their migration through open ocean to 'home' and nest at isolated spots such as Ascension Island (AI) in the mid-Atlantic (see also [2]). Journeys of this nature are not uncommon in the animal kingdom, with other notable examples being the pole-to-pole migrations of Arctic terns and the return of mature salmon to spawn at natal grounds. Uncovering the cues that provide the necessary orienteering information—celestial, geomagnetic, topographic, chemical, etc.—is a key concern: determining the mechanistic basis for navigation sheds light on challenging ecological questions, such as the impact of environmental change on populations (e.g. [3]).

A complicating factor is the flow in the surrounding medium, from ocean and river currents for aquatic organisms to wind for airborne populations [4–6]. Flow can be benevolent or malevolent: on the one hand, movement is energetically demanding and currents provide a useful conveyor belt; on the other, a powerful current or storm could transport population members into inhospitable or unfamiliar environments. Whether they assist or hinder, effective navigation clearly demands a finely tuned navigational system capable of correcting or compensating for currents [6].

Understanding these processes requires integration and interpretation of various data sources. Ocean currents and air movements can be obtained from direct measurements or hydrodynamic models. Regarding navigation, recent years have led to the wide-scale adoption of GPS-based telemetry for tracking animal movements at global scales and over inaccessible environments. Datasets are immense, yet allow paths to be evaluated in terms of key statistical quantities, including average speeds, turning rates and angles. Coupled to controlled behavioural studies and knowledge of the flows encountered, we are certainly better equipped to understand the basics of navigation.
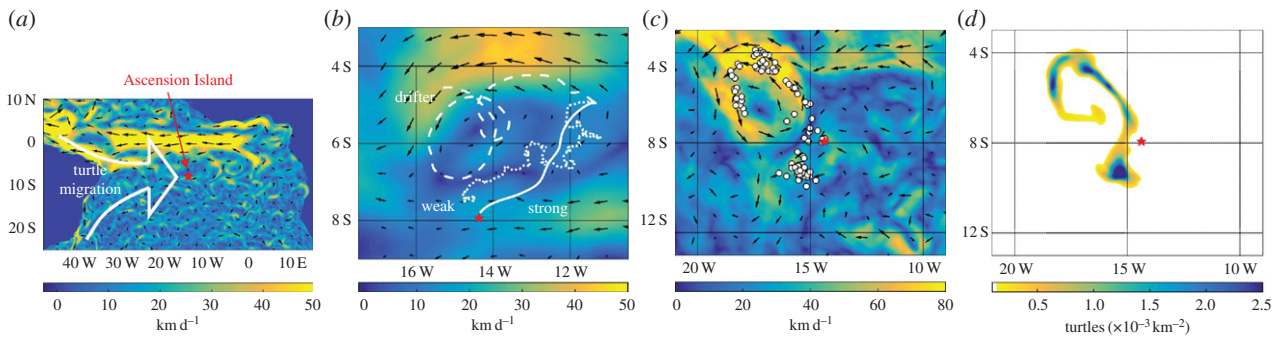
Figure 1. (a) Adult green turtles migrate from coastal South America to nest at AI (ocean current velocity indicated by scale and arrows, averaged over January 2014). (b) IBM simulations. Simulated paths over 50 days following an individual's displacement from AI (star), where the individual acts as a drifter, a weak or a strong navigator: only the latter reaches AI within the simulation time; the displayed ocean currents are averaged over the 50 day period. (c,d) Population distribution snapshot of the (c) IBM and (d) continuous model (75 days post-release): simulation details in figure 7. (Online version in colour.)

1.1. Modelling movement in ecology

Despite advances in data acquisition, field studies remain difficult and costly and the complementary use of modelling has become commonplace: modelling provides a framework through which hypotheses can be tested and the impact of perturbations simulated. Access to powerful computing has led to a marked increase in the use of individual-based models (IBMs), where each population member is tracked as it moves through its environment [7]. The adaptability of IBMs is clearly to their advantage, generating tailor-made data that can be fitted/validated against experimental sources.

For organisms in a fluid environment, a typical approach is to 'immerse' an IBM into an imposed flow, so that self-propelled movement becomes augmented by the flow. Lagrangian-based particle models are often employed for the IBM, with each individual indexed by its instantaneous position and velocity: navigation can be incorporated via a directional bias according to orienteering cues. Currents can be obtained from widely available datasets and models based on these principles have been applied to understand movement dynamics across aquatic and airborne populations: the advection-dominated movement of fish larvae [8]; the role of current-directed movement in jellyfish blooms [9]; the influence of directed movement on turtle drifting within ocean currents [10,11]; the Atlantic movements of eel larvae [12]; how wind influences the choice of staging sites during red knot migration [13]; the exploitation of favourable winds by high-flying insects [14]. For many further references and examples, see [15,16].

Assessing a strategy's effectiveness demands some measure and a standard approach is to define 'Lagrangian targets', against which simulation output can be evaluated [15]: for example, what proportion of a population reach some place (e.g. a spawning site) by some time (e.g. the spawning season)? Yet given that an individual's path is subject to significant intrinsic (e.g. imprecision in the navigating mechanism) and extrinsic (e.g. turbulence of currents) variability, care must be paid to the number of simulated organisms for meaningful information to be drawn. Coupled to their limited analytical tractability, it can become hard to draw broad insights from IBMs without recourse to computationally demanding simulations.

An alternative is to propose a fully continuous and macroscopic model, for example via an equation for the population density: for movement within a flowing medium, partial differential equations (PDEs) based on systems of diffusion–advection–reaction equations would be a natural choice.

With their roots in classical applied mathematics, they yield to analytical investigation and are typically efficient to solve numerically. In the present context, PDE models have been used in problems ranging from predicting tuna distributions [17] to the persistence of stream populations in the face of fast currents [18] and the dispersal of moths [19].

Weighed against their analytical tractability, continuous models prove problematic with respect to parametrization and validation against individual-level data. Consequently, a third route is to formally connect an IBM with a PDE model via some scaling-based approach: by drawing clear lines between the data-friendly IBM and the terms and parameters of a macroscopic model, their distinct advantages can be exploited. We refer to [20,21] for recent reviews with regards to biological movement; in the context of the present article, we particularly mention [22,23].

1.2. Outline

The main aim here is to model organism movement in a flowing field: see figure 1 for a schematic. We follow the standard protocol for the IBM by immersing a Lagrangian-based particle model into a flowing medium. The IBM confers a navigating capacity, with individuals orienting according to spatially and temporally varying cues. Section 2 summarizes this model and the scaling methods that yield a macroscopic continuous model for the population density, which is of drift-anisotropic diffusion form. In §3, we tailor this approach to certain movement classes, including passive drifters and active navigators. Sections 4 and 5 consider an expository application to homing behaviour, beginning with an idealized scenario and followed by a preliminary data-driven study into green turtle homing to AI. Numerical simulations confirm the method's validity, highlighting its capacity to generate data at both an individual and population level. Moreover, the continuous model's greater tractability is exploited, demonstrated via the use of characteristics to quantify the 'navigational strength' required by organisms: if the internal compass is too weak, individuals fail to home.

2. Individual and continuous models

2.1. The individual-based model

Each individual is a point particle exerting negligible effect on the surrounding flow, with the position of the ith individual

denoted by $\mathbf{x}_i \in \mathbb{R}^n$ (n is the space dimension). Positional changes are due to (i) *passive movement* (the external flow) and (ii) *active movement* (swimming/flight). Generally, $n = 3$, since organisms move freely in three-dimensional space; however $n = 2$ is often sufficient: for example, many oceanic populations spend the majority of their time at the same depth.

For passive movement, we define $\mathbf{u}(t, \mathbf{x}) \in \mathbb{R}^n$ as the medium flow at time t and position $\mathbf{x}$. Active movement follows a velocity-jump random walk [24], in which smooth runs through space with a constant *active velocity* $\mathbf{v} \in \mathbb{R}^n$ are punctuated by 'turning' and new velocity selection. Turning is regarded as instantaneous and the time between successive turns assumed to follow a Poisson distribution, with (constant) turning rate parameter λ. The new active velocity is selected from a distribution $q(\mathbf{v}|t, \mathbf{x})$ and can incorporate orienteering: navigating cues enter via a bias into specific active velocities. We implicitly assume that the previous active velocity has no impact on the new active velocity, although this can be accounted for by extending to $q(\mathbf{v}|t, \mathbf{x}, \mathbf{v}')$ for previous velocity $\mathbf{v}'$.

Mathematically, if individual i is at position $\mathbf{x}_i(t)$ and has active velocity $\mathbf{v}_i(t)$ at time t, then at time $t + \Delta t$ (assuming Δt is sufficiently brief), we have

$$\mathbf{x}_i(t + \Delta t) = \mathbf{x}_i(t) + \Delta t(\mathbf{v}_i(t) + \mathbf{u}(t, \mathbf{x}_i));$$

$$\mathbf{v}_i(t + \Delta t) = \begin{cases} q(\mathbf{v}|t + \Delta t, \mathbf{x}_i(t + \Delta t)) & \text{with probability } \lambda \Delta t, \\ \mathbf{v}_i(t) & \text{otherwise.} \end{cases}$$
(2.1)

Here, we assume individuals move with the same fixed *active swimming/flight speed*, s: only a new active direction is chosen at a turn. This simplification reduces burdensome parameters and allows us to set $\mathbf{v} = s\mathbf{n}$, where $\mathbf{n} = \mathbf{v}/|\mathbf{v}|$ is the unit vector describing the active direction. The distribution q over velocity space V can be redefined as a directional distribution $\tilde{q}$ over all possible directions (i.e. on the unit sphere, $\mathbb{S}^{n-1}$):

$$q(\mathbf{v}|t, \mathbf{x}) := \frac{\tilde{q}(\mathbf{n}|t, \mathbf{x})}{s^{n-1}}$$
(2.2)
$$\text{for active direction } \mathbf{n} = \mathbf{v}/|\mathbf{v}| \in \mathbb{S}^{n-1}.$$

2.2. The continuous model

Model (2.1) offers an individual-level model of movement at a 'mesoscopic' scale. Many navigational problems, however, play out for large populations at macroscopic scales: green turtles take weeks to migrate to breeding grounds thousands of kilometres away. Simulating IBMs can be costly at these larger scales and obtaining an equation for the population density distribution, $m(t, \mathbf{x})$, becomes attractive.

The process for doing so is intricate yet relatively commonplace: we therefore leave details in the electronic supplementary material and refer to [21]. In brief, we first propose a continuous, mesoscopic formulation of the IBM (the 'transport model') and then apply scaling to derive the macroscopic equation for $m(t, \mathbf{x})$. This takes the form of the drift-anisotropic diffusion model:

$$m(t, \mathbf{x})_t + \nabla \cdot ((\mathbf{a}(t, \mathbf{x}) + \mathbf{u}(t, \mathbf{x}))m(t, \mathbf{x}))$$
$$= \nabla\nabla(\mathbb{D}(t, \mathbf{x})m(t, \mathbf{x})).$$
(2.3)

Here, $\mathbf{u}(t, \mathbf{x})$ is the previously defined external flow while the advective velocity, $\mathbf{a}(t, \mathbf{x})$, and anisotropic diffusion tensor,

$\mathbb{D}(t, \mathbf{x})$, derive from the active movement. Specifically, they relate to statistical properties of the turning distribution:

$$\mathbf{a}(t, \mathbf{x}) = \int_V \mathbf{v}q(\mathbf{v}|t, \mathbf{x})\mathrm{d}\mathbf{v},$$
$$= s \int_{\mathbb{S}^{n-1}} \mathbf{n}\tilde{q}(\mathbf{n}|t, \mathbf{x})\mathrm{d}\mathbf{n};$$
(2.4)
$$\mathbb{D}(t, \mathbf{x}) = \frac{1}{\lambda} \int_V (\mathbf{v} - \mathbf{a}(t, \mathbf{x}))(\mathbf{v} - \mathbf{a}(t, \mathbf{x}))^T q(\mathbf{v}|t, \mathbf{x})\mathrm{d}\mathbf{v},$$
$$= \frac{1}{\lambda} \int_{\mathbb{S}^{n-1}} (s\mathbf{n} - \mathbf{a}(t, \mathbf{x}))(s\mathbf{n} - \mathbf{a}(t, \mathbf{x}))^T \tilde{q}(\mathbf{n}|t, \mathbf{x})\mathrm{d}\mathbf{n}.$$
(2.5)

In other words, $\mathbf{a}$ is the direction of an 'average' swimmer, encoded in the underlying directional distribution, while the diffusion tensor derives from the inaccuracies stemming from directional choice. Formally, $\mathbf{a}(t, \mathbf{x})$ is the expectation and $\mathbb{D}(t, \mathbf{x})$ is $1/\lambda$ multiplied by the variance–covariance matrix of q. Consequently, the macroscopic equations depend explicitly on two statistical quantities that can be drawn from observations of individual movement.

Equation (2.3) is a parabolic differential equation, yet it can still be useful to study the characteristics of the net flow field. Doing so offers a continuous path back to individual detail: they can be interpreted as equations of motion for an 'average' individual and their (relatively) simple form is analytically amenable. For (2.3), we have

$$\frac{\mathrm{d}\mathbf{x}}{\mathrm{d}t} = \mathbf{u}(t, \mathbf{x}) + \mathbf{a}(t, \mathbf{x}) - \nabla \cdot \mathbb{D}(t, \mathbf{x}).$$
(2.6)

We use this equation later to derive a condition for successful navigation towards a target (see §4.4.2).

3. Drifters to navigators

Our framework accounts for various movement classes and we tailor it for the following:

— *Drifters*—particles without active motion that simply move with the flow of the surrounding medium.
— *Random movers*—self-propelled organisms with negligible orientating bias in their movement paths (at the level of observation).
— *Navigators*—self-propelled organisms showing biased movement paths, generated from following navigating cues.

Here, we restrict to two-dimensional scenarios, relevant to aquatic (airborne) populations that *predominantly* swim (fly) at the same depth (height): movements through the depth column occur, but are assumed negligible over the time and space scales considered. For example, while occasional deeper dives (to around 10–20 m) occur, tracking of green turtles indicates that most swimming is at or near the surface [25]. We note that the extension to three dimensions is relatively straightforward, yet is beyond the aims and applications of this paper. For two dimensions, we consider a polar coordinate system: velocities are given by $\mathbf{v} = s\mathbf{n} = s(\cos\alpha, \sin\alpha)$ where $\alpha \in [0, 2\pi)$ is the angle corresponding to direction $\mathbf{n}$. For the turning response, we specify a circular distribution, $\tilde{q}(\alpha)$.

3.1. Movement classes
3.1.1. Drifters
A pure drifter is a particle without active movement. Few organisms are truly drifters (e.g. ballooning spiders), yet

4

various studies approximate as such if active movement is believed negligible compared to the flow (e.g. [12]). Drifters simply correspond to zero speed, $s = 0$, and expressions (2.4) and (2.5) are zero, regardless of the turning distribution. The macroscopic model is a pure drift equation due to the medium flow:

$$m(t, \mathbf{x})_t + \nabla \cdot \mathbf{u}(t, \mathbf{x})m(t, \mathbf{x}) = 0. \tag{3.1}$$

3.1.2. Random movers

Organisms with self-propulsion but no orientation undergo an unbiased Pearson random walk [24]: an individual moves some distance in one heading before selecting a new one, favouring all new directions equally. Consequently, we consider in this case the uniform turning distribution:

$$\tilde{q}(\alpha) = \frac{1}{2\pi}.$$

Substituting into (2.4) and (2.5) and integrating yields

$$\mathbf{a}(t, \mathbf{x}) = \mathbf{0} \quad \text{and} \quad \mathbb{D}(t, \mathbf{x}) = \frac{s^2}{2\lambda}\mathbb{I}_2.$$

In the above, $\mathbb{I}_2$ is the 2×2 identity matrix and we obtain a drift-(isotropic) diffusion equation in the macroscopic model:

$$m(t, \mathbf{x})_t + \nabla \cdot \mathbf{u}(t, \mathbf{x})m(\mathbf{x}, t) = d\nabla^2 m(t, \mathbf{x}), \tag{3.2}$$

where the diffusion coefficient $d = s^2/(2\lambda)$.

3.1.3. Navigators

In practice, most organisms receive navigating information from their environment. We can account for guidance cues through biasing the turning distribution: an external cue is assumed to guide individuals in some dominant direction, denoted by the unit-length vector $\mathbf{w}(t, \mathbf{x}) \in \mathbb{R}^n$, with bias parameter $k(t, \mathbf{x}) \geq 0$. $k(t, \mathbf{x})$ measures the *navigational strength* and indicates the directional accuracy: at $k = 0$, the choice is random (and we recover a random mover); increasing k allows the dominant direction to be chosen with increasing accuracy, culminating in 'perfect navigation' when the dominant direction is always selected. $k(t, \mathbf{x})$ and $\mathbf{w}(t, \mathbf{x})$ are expected to be position and time dependent, assuming spatio-temporal variation in the intensity and direction of a navigating cue. Further, these parameters can also be chosen to explicitly depend on some factor, such as the geomagnetic field or chemical signals. For clarity of presentation, we drop these notational dependencies in the following.

In two dimensions, we consider a distribution on the unit circle. The von Mises distribution, as a circular analogue to the normal distribution, offers a de facto standard for describing directional datasets and has been widely adopted in the analysis and modelling of animal navigation (e.g. [21,26–29]). In circular coordinates, we choose $\mathbf{w} = (\cos A, \sin A)$, where $A(t, \mathbf{x})$ defines the dominant angle, and the von Mises distribution is given by

$$\tilde{q}(\alpha | k, A) = \frac{1}{2\pi I_0(k)} e^{k \cos(\alpha - A)}. \tag{3.3}$$

$I_j(k)$ denotes the modified Bessel function of first kind (and of order j). Here, $k(t, \mathbf{x}) \in [0, \infty)$, where $k = 0$ corresponds to zero bias and $k \to \infty$ yields perfect navigation. From

(2.4)–(2.5) (see [21]), we find

$$\mathbf{a}(k, A) = s\frac{I_1(k)}{I_0(k)}(\cos A, \sin A),$$

$$\mathbb{D}(k, A) = \frac{s^2}{2\lambda}\left(1 - \frac{I_2(k)}{I_0(k)}\right)\begin{pmatrix} 1 & 0 \\ 0 & 1 \end{pmatrix}$$

$$+ \frac{s^2}{\lambda}\left(\frac{I_2(k)}{I_0(k)} - \frac{I_1(k)^2}{I_0(k)^2}\right)\begin{pmatrix} \cos^2 A & \cos A \sin A \\ \cos A \sin A & \sin^2 A \end{pmatrix}. \tag{3.4}$$

The active advection is in the same direction as the dominant direction, whereas the diffusion tensor is split into isotropic and anisotropic components, where the anisotropy also depends on A.

Finally, we remark that for instances of multiple preferred directions, e.g. competing orienteering cues, we can choose a turning distribution composed from linear combinations of (3.3). Subsequently, advection and diffusion terms will come from linear combinations of (3.4).

3.2. Data to macroscopic measures

We demonstrate the von Mises distribution via converting data into macroscopic measures for theoretical and genuine populations (figure 2a). In the top row, we consider a population with no dominant orientation, while a genuine dataset is shown in the bottom row: the swimming orientation of juvenile green turtles (*Chelonia mydas*) exposed to magnetic fields encountered during ocean travels (reproduced from fig. 2 of [30], 'Northern Field' dataset).

Standard methods (e.g. [26]) are used to estimate k and A in (3.3), shown in figure 2b. For the non-oriented population, k is negligible and the distribution quasi-uniform. The genuine dataset, however, yields a large k: this indicates a clear bias in turtle orientation, suggesting a response to the magnetic field. Calculations for similar datasets reported in [30–32] also reveal clear orientational biases, with $k \sim 0.5 - 2$. Of course, one should be cautious in subsequent applications of controlled laboratory based data to real-world navigation problems.

Figure 2c illustrates advective velocities (**a**) and diffusion tensors ($\mathbb{D}$), calculated from (3.4). The former are represented via the arrow lengths and directions; the maximum length is s (outer dotted circle) and occurs for 'perfect navigation'. Diffusion tensors are exemplified by ellipses indicating the diffusion in distinct axial directions. The quasi-uniform distribution yields negligible advection and almost isotropic diffusion. Oriented distributions generate large advective velocities in the dominant direction with reduced and anisotropic diffusion: greatest orthogonal and lowest along the axial direction of bias, due to limited movement against the dominant direction.

Simulations of the macroscopic model (2.3) are shown in figure 2d under these forms (setting $s = \lambda = 1$). The unbiased dataset generates a population that diffuses in quasi-isotropic fashion, while the oriented population is advected along the dominant direction; note the 'stretching' due to anisotropic diffusion.

4. Goal navigation under fixed external flows

We demonstrate the methods within a precise application: how does external flow impact on navigation/homing to a goal? Such problems occur in numerous examples, from pheromone
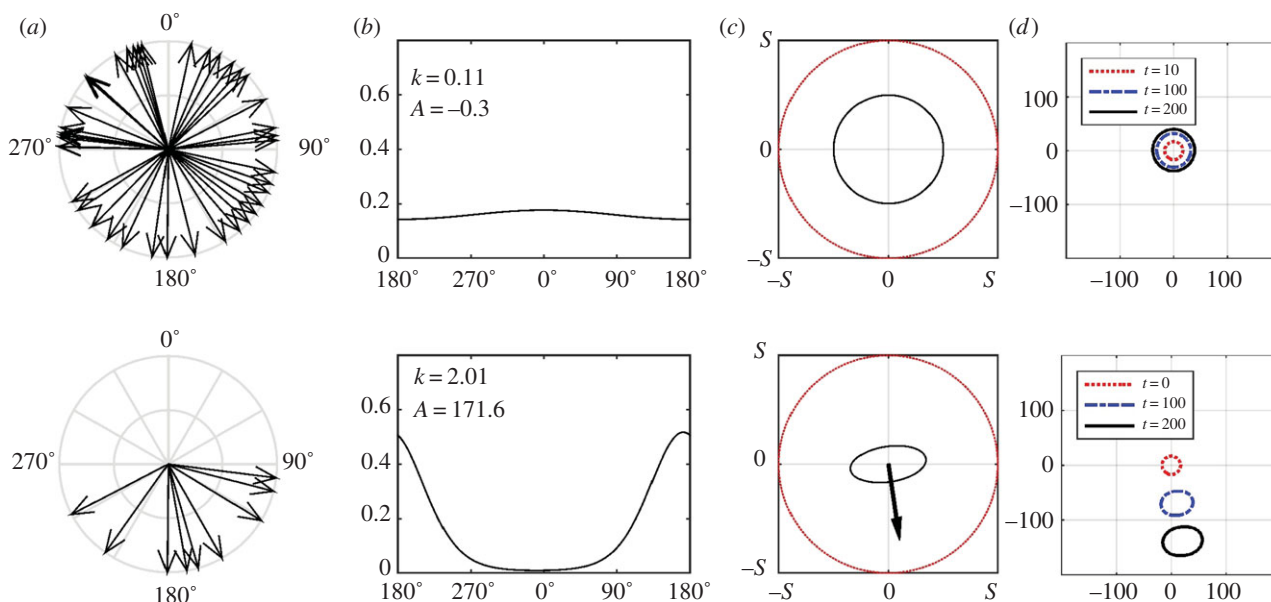
Figure 2. Translation from circular datasets to macroscopic terms for (top) unbiased and (bottom) biased populations. (a) Datasets, with each angular entry indicated by an arrow; (b) von Mises distribution (3.3) and its two defining parameters; (c) advective velocity (**a**) and diffusion tensor ($\mathbb{D}$) representations, calculated from equation (3.4); (d) simulations of equation (2.3). For simulations, we plot the contour line of constant density ($=10^{-4}$) at successive times for a population initiated at the origin. (Online version in colour.)

following by moths to adult marine turtle homing. We begin with a simple scenario, where a generic population attempts to navigate to some goal under a fixed and uniform flow. While idealized, this could perhaps be interpreted as a hypothetical experiment, where a population's movement is studied in a tank or wind tunnel under a controlled flow, or as an approximated description of a river environment with a (relatively) steady flow. The principal aim is to explore whether the continuous model captures population-level detail of the IBM and investigate the critical navigational strength for successful homing; we note that a study under naturally occurring flows is performed in the next section.

4.1. Region and initial conditions

We suppose movement occurs within a two-dimensional rectangular arena, $(x, y) \in [-L_x, L_x] \times [-L_y, L_y]$, and denote x- and y-axes as 'west to east' and 'south to north', respectively. We assume $(0,0)$ marks the centre of the intended goal, which forms a circular region of diameter 10, for example, an island for turtle navigation.

At the edges, we assume no-loss boundary conditions: individuals leaving the arena are instantaneously 'reflected'. In practice, the arena is larger than the region where the principal dynamics are taking place, so that edge effects have relatively little impact: exploratory simulations with other boundary conditions (e.g. absorbing) demonstrate the same general behaviour.

We consider two forms of initial condition for a population of N individuals.

(1) *Localized release*. These simulate a 'mark and release' study, with individuals released from a given location. For the IBM, an initial location is drawn from a bivariate normal distribution with mean position (x_0, y_0) and symmetric variances σ^2. In the macroscopic model, this translates to initial conditions of the form

$$m(x, y, 0) = \frac{N}{2\pi\sigma^2} \exp\left\{ -\frac{(x-x_0)^2 + (y-y_0)^2}{2\sigma^2} \right\}.$$

(2) *Uniform distribution*. The population is uniformly distributed over a circle of radius R. For the macroscopic model, we set

$$m(x, y, 0) = \begin{cases} \dfrac{N}{\pi R^2} & \text{if } x^2 + y^2 \leq R^2 \\ 0 & \text{otherwise.} \end{cases}$$

Initial active velocities for the IBM are selected from the turning distribution for active movement, based on their initial location. Numerical methods have been adapted from those developed previously [29] and details are in the electronic supplementary material.

4.2. Active and passive movement parameters

Passive movement results from a uniform and constant external flow from west to east: we set $\mathbf{u} = (u_x, 0)$ where $u_x \geq 0$. A generic cue navigates individuals towards the goal: we take the von Mises distribution (3.3), with an individual at $\mathbf{x} = (x(t), y(t))$ experiencing a bias in the dominant direction $\mathbf{w} = -\mathbf{x}/|\mathbf{x}|$. For simplicity, we set $k(x, y, t) = \text{const.}$: the cue exerts a uniform navigational strength. In practice, we expect the cue's strength to vary, but leave these considerations for future studies.

We take a dimensionless form, with mean active speed and turning rates fixed and scaled to unit values: $s = \lambda = 1$. This allows us to focus on the flow (u_x) and navigational strength (k). Specifically, we assume $0 \leq u_x \leq s$ so that the flow is between 0 and 100% of an individual's active speed: our framework also allows external currents to exceed the individual's active speed, as happens in the later application to AI homing. We take $k \in [0, 3]$: upper end values generate more than half of the turns within $\pm 25°$ of the goal's true bearing, whereas at $k = 0.5$ this drops to a quarter; estimates of k from the datasets in [30–32] all fall comfortably inside this range.

Simulations of the IBM are conducted for $t \in [0, 1000]$ and initial conditions:

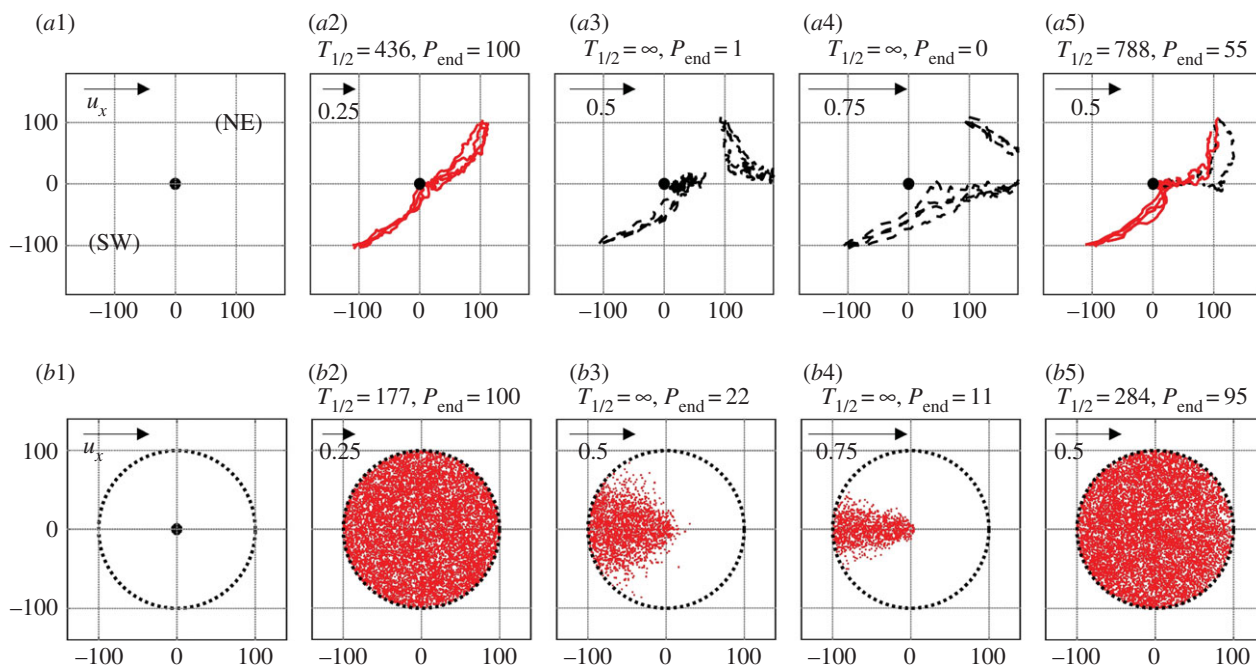(SW) A localized release at $(x_0, y_0) = (-100, -100)$ ($\sigma = 5$), southwest and up-current of the goal.

6

Figure 3. Simulations of the IBM under different initial conditions. (*a*1) 'Release' set-up, illustrating release locations relative to the goal (central dot). (*a*2–*a*5) Representative tracks for (*a*2) $u_x = 0.25$, $k = 1.0$, (*a*3) $u_x = 0.5$, $k = 1.0$, (*a*4) $u_x = 0.75$, $k = 1.0$ and (*a*5) $u_x = 0.5$, $k = 1.5$. Successful (solid red lines) and unsuccessful (black dashed) tracks are differentiated. The direction and flow strength are indicated by the top left arrows, while measures P_{1000} and $T_{1/2}$ are given above each plot. (*b*1) 'Uniform' set-up with individuals distributed across the circular region surrounding the goal (central dot). (*b*2–*b*5) Initial locations of individuals that reach the goal by $t = 1000$ are marked by red dots for (*b*2) $u_x = 0.25$, $k = 1.0$, (*b*3) $u_x = 0.5$, $k = 1.0$, (*b*4) $u_x = 0.75$, $k = 1.0$ and (*b*5) $u_x = 0.5$, $k = 1.5$. Note that we only show the centre of the full region, where $L_x = L_y = 300$. (Online version in colour.)

(NE) A localized release at $(x_0, y_0) = (+100, +100)$ $(\sigma = 5)$, northeast and down-current of the goal.

(UD) A uniform distribution over the circle of radius $R = 100$ surrounding the goal's centre.

Population success is assessed via two Lagrangian targets: P_{1000}, the population percentage that reaches the goal by $t = 1000$; and $T_{1/2}$, the time half the population has reached the goal ($T_{1/2} = \infty$ if this is not achieved by $t = 1000$).

To exemplify this within a dimensional context, consider an organism that swims with a mean speed 1 km h^{-1} and mean turning rate 1 h^{-1}. Then (under SW or NE), our individuals are initially released just over 140 km from a goal of diameter 10 km, and we study their movement paths over a period of about six weeks.

4.3. Individual-based model simulations

We release 1000 individuals SW or NE of the goal (figure 3*a*1). Figure 3*a*2–*a*4 shows representative trajectories for $k = 1$ and: (*a*2) a weak flow (25% of the individual's maximum speed); (*a*3) a moderate flow (50%); and (*a*4) a strong flow (75%). For weak flows, all individuals find the goal by $t = 1000$ regardless of release location, although (unsurprisingly) those initially down-current experience a delayed passage. A critical transition occurs for moderate and strong flows, with only a few reaching the goal for the former and none for the latter: the current is too strong and most are swept away. For moderate flows, increasing the bias parameter to $k = 1.5$ drastically increases the population's success (figure 3*a*5).

We next consider a population ($N = 10\,000$) distributed according to UD (figure 3*b*1). Figure 3*b*2–*b*5 shows initial locations of individuals that succeed in reaching the goal, for various (u_x, k) combinations. Failure increases as the external flow increases: for moderate/strong flows, only a small upstream sector with advantageous initial locations succeed.

Increasing k to 1.5 for the moderate flow again drastically increases population success (figure 3*b*5).

4.4. Continuous simulations

4.4.1. Individual-based model and macroscopic model comparison

The simulations hint at a sharp population success/failure transition, depending on flow and navigational strength parameters. Can we exploit the macroscopic model to investigate this systematically? Population densities drawn from the IBM are compared with $m(t, \mathbf{x})$, computed from (2.3), under an identical scenario, with a typical result given in figure 4*a,b*. An excellent quantitative match is observed between the individual and continuous models: other comparisons produce similar results. We conclude that, for the time and space scales considered, the macroscopic model recapitulates population distributions of the IBM.

We hence exploit the numerical advantage of (2.3) to investigate population success as we sweep through parameter space. Figure 5*a* plots P_{1000} for the three initial distributions: SW; NE; and UD. As expected, high navigational strength allied to slow flows permits easy goal navigation.

4.4.2. Critical navigating strength

Results in figure 5*a–c* reinforce the notion of a critical success/failure transition and we quantify this by analysing equations (2.6). For the problem at hand, we obtain $\mathbb{D}$ and $\mathbf{a}$ from (3.4) and take $\mathbf{u} = (u_x, 0)$. Full details are shown in appendix A, where we obtain the dynamical system

$$\left.\begin{aligned} \dot{x} &= u_x - c_1 \frac{x}{\sqrt{x^2 + y^2}} - c_3 \frac{x}{x^2 + y^2} \\ \text{and} \quad \dot{y} &= -c_1 \frac{y}{\sqrt{x^2 + y^2}} - c_3 \frac{y}{x^2 + y^2}. \end{aligned}\right\} \tag{4.1}$$
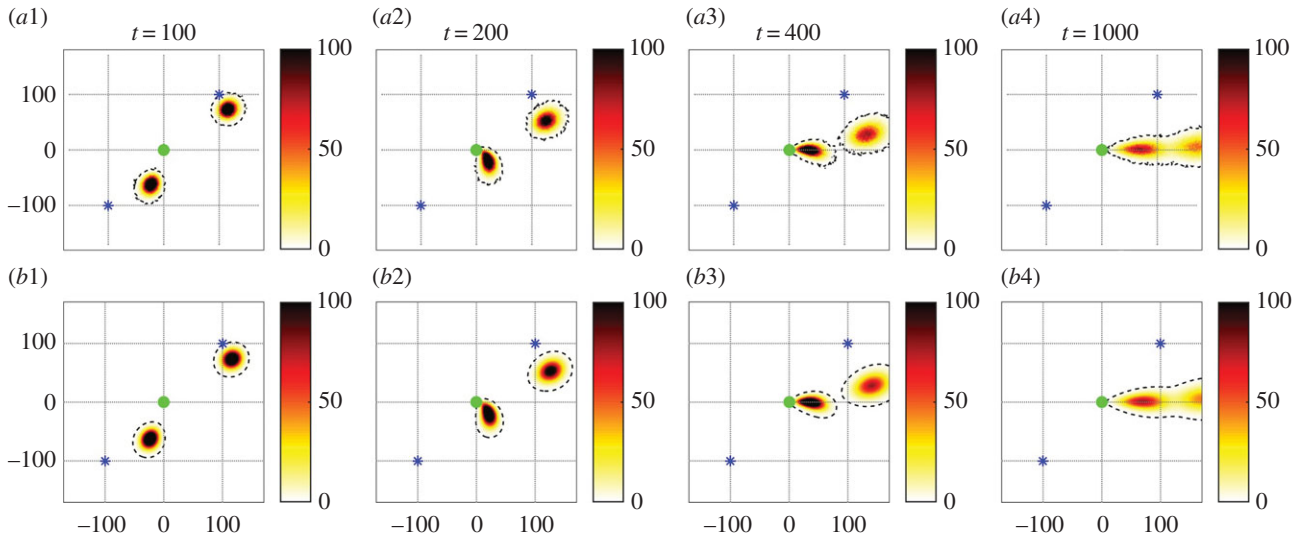
Figure 4. Comparison between (*a*) the IBM and (*b*) the macroscopic model. A total of 100 000 individuals are released both NE and SW (stars) from the goal (circle); here, $u_x = 0.5$, $k = 1$ and other parameters as defined in the text. (*a*) IBM. Positions are binned into a two-dimensional histogram to generate a population density map, plotted at the times indicated. (*b*) Macroscopic model. We numerically solve (2.3) according to the parameters and initial conditions of the IBM, with macroscopic terms computed from (3.4). Population densities are indicated by the density scale and a dashed-black curve for the constant density contour line (=1). (Online version in colour.)
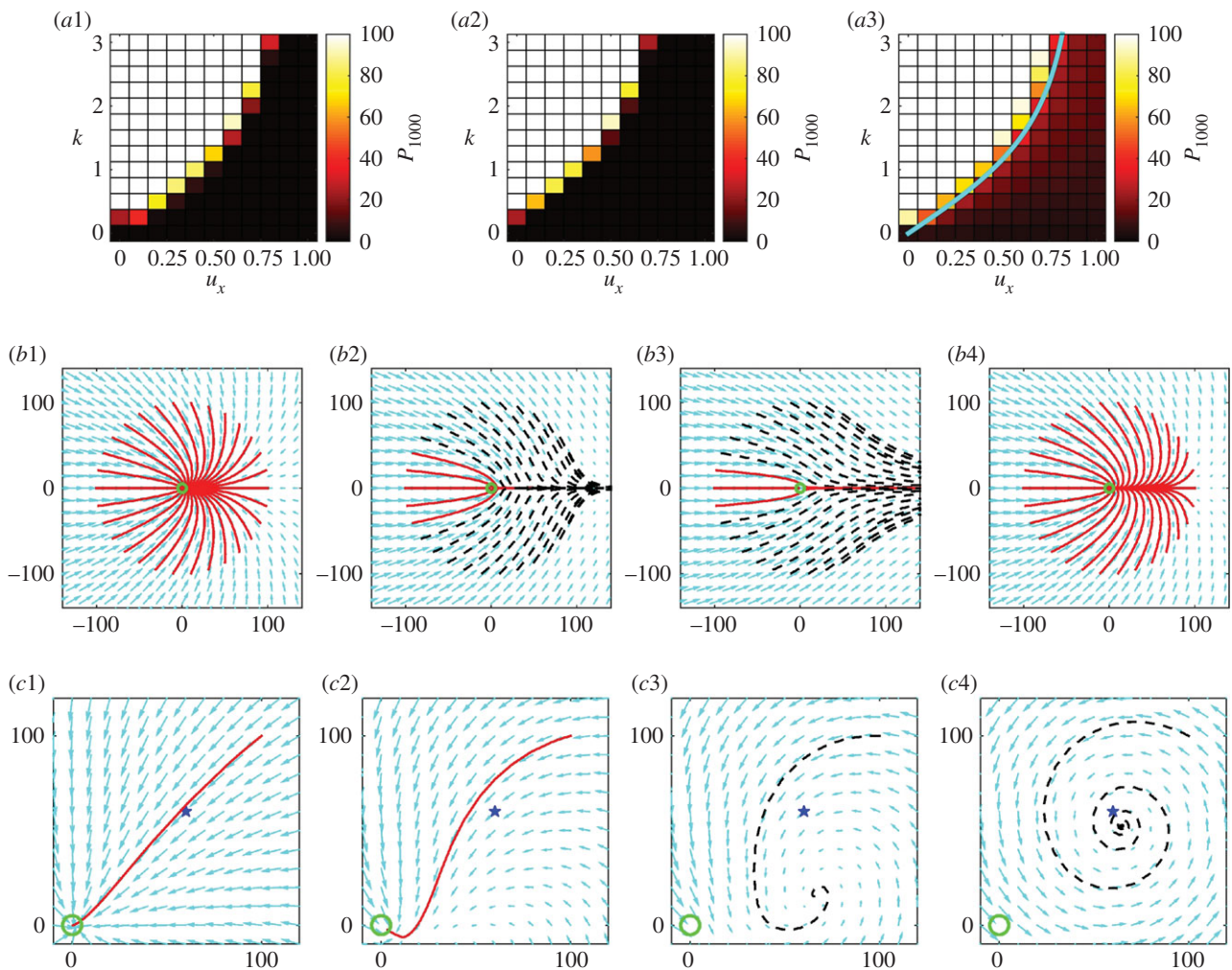

Figure 5. Navigating success and the use of characteristics. (*a*) Population success (measured via P_{1000}) over a range of parameter combinations and for initial distributions (*a*1) SW, (*a*2) NE and (*a*3) UD. In (*a*3), the curve (thick line) determined from (4.2) is overlaid. (*b*) Trajectories of (4.1) for the scenario described in figure 3*b*; trajectory initial conditions placed on the ring of radius 100. Here, $s = \lambda = 1$ and: (*b*1) $u_x = 0.25$, $k = 1.0$; (*b*2) $u_x = 0.5$, $k = 1.0$; (*b*3) $u_x = 0.75$, $k = 1.0$; (*b*4) $u_x = 0.5$, $k = 1.5$. (*c*) Trajectories for a whirlpool scenario. The trajectory beginning at (100, 100) is shown for equations (4.3) with $s = \lambda = k = 1$ and whirlpool strengths: (*c*1) $\gamma = 0.001$; (*c*2) $\gamma = 0.005$; (*c*3) $\gamma = 0.01$; (*c*4) $\gamma = 0.05$. In (*b*,*c*), successful (solid line) and unsuccessful (dashed line) orbits are shown according to whether they pass through or miss the goal (circle). Small arrows indicate the directional field of the characteristic equations, while stars in (*c*) indicate the whirlpool centre. (Online version in colour.)

Coefficients c_1 and c_3 are given in equations (A 1) of appendix A and depend on k (noting $s = \lambda = 1$).

We test whether (4.1) adequately describes the movement process by computing and comparing its trajectories with the scenario of figure 3b: trajectories in figure 5b1–b4 are differentiated according to whether they hit (solid red) or miss (dashed black) the goal; the small arrows illustrate the *net* flow field of (4.1), derived from the external flow **u**, the active orientation **a** and diffusion gradient. Compared against figure 3b, we clearly observe excellent qualitative and quantitative agreement.

Given this quantitative match, we conclude that (4.1) closely describes the average individual behaviour and use stability analysis (see appendix A) to obtain the following approximate[1] condition for population success:

$$s \frac{I_1(k)}{I_0(k)} > u_x. \tag{4.2}$$

The left-hand side increases with k, saturating to s. For a given flow, (4.2) provides a quantitative estimate for the necessary navigational strength: the guiding signal must be strong enough to compensate for the flow; moreover, navigation is unsuccessful for $u_x > s$. We overlay this condition on the results from parameter sweeps in figure 5a3: it clearly delineates the regions between success and failure.

We have concentrated on steady/uniform flows, yet the characteristic equations can also be applied to the non-trivial flows often found in nature. As an example, we set $\mathbf{u} = \gamma(66 - 0.1x - y, x - 0.1y - 54)$ and the new characteristic equations become

$$\left.\begin{aligned} \dot{x} &= \gamma(66 - 0.1x - y) - c_1 \frac{x}{\sqrt{x^2 + y^2}} - c_3 \frac{x}{x^2 + y^2} \\ \text{and} \quad \dot{y} &= \gamma(x - 0.1y - 54) - c_1 \frac{y}{\sqrt{x^2 + y^2}} - c_3 \frac{y}{x^2 + y^2}. \end{aligned}\right\} \tag{4.3}$$

This creates a 'whirlpool', swirling anticlockwise towards the point (60,60) and at a rate determined by γ. In figure 5c, we consider trajectories of (4.3), starting from (100,100) and with active navigation to the goal. For figure 5c1–c4, we increase the whirlpool's strength: if weak, trajectories hit the goal (figure 5c1,c2), yet when stronger they are sucked into the whirlpool (figure 5c3,c4); note that the convergence points do not coincide exactly with the whirlpool centre, due to the active movement.

5. Natal homing to Ascension Island by green turtles

As illustrated by figure 5c, complicated currents can heavily impact on movement paths and we move to a genuine, data-driven application: the homing of green turtles (*C. mydas*) to AI, a volcanic island of less than 100 km^2 and more than a 1000 km from the nearest landmass (figure 1a).

Adult turtles make this journey once every few years [33], travelling over 2000 km from South American waters to nest at their natal beach (figure 1a). Nesting starts December/January and continues through to June/July [34], with many females laying multiple clutches [33]. How this navigational feat is accomplished remains an outstanding question and various theories have been proposed, from following odours emanating from the island [35] to geomagnetic field orientation [36]. In this expository study, we focus neither

on the full journey nor the precise navigating mechanism, rather we test our methodology and examine the ease of finding the island inside the final few hundred kilometres. For further theories on marine turtle navigation, see [2,37].

5.1. Region and initial conditions

AI lies approximately 7°57′ S and 14°22′ W and we set this as the centre of our region. We say that simulated turtles successfully reach the island if they arrive within 15 km of its centre (approx. 10 km from its coastline): at this distance, we assume short-range cues (e.g. sound or smell based) lead them to the island. Initially, we apply controlled releases at locations ($\pm 3°$, $\pm 3°$) northeast (NE), southeast (SE), southwest (SW) and northwest (NW) of the goal (simulating mark and release experiments). As before, our plots focus on a compact region centred on the island, yet simulated turtles move within an extended region (with no-loss boundary conditions).

The initial time is set early in the nesting season: most simulations use a start date of 1 January 2014 (according to ocean current data) and this is defined as 'time zero'; later releases are indicated by $+X$ days. Simulations are performed for 150 days, corresponding to a time towards the end of the nesting season.

5.2. Passive movement: ocean flow data

Ocean flows can be obtained from a variety of sources: here, we use data (downloaded from http://pdrc.soest.hawaii.edu/data/data.php) provided by global HYCOM (the global Hybrid Coordinate Ocean Model [38]), an ocean forecasting model forced by factors such as wind speed and heat flux and assimilated with measurements from satellites, floats, moored buoys, etc. to yield 'hindcast' model output. HYCOM has a spatial resolution capable of reproducing both large-scale currents and localized (temporally and spatially) phenomena such as meandering currents and eddies: potentially significant for turtle navigation to a small island. In its application, we linearly interpolate HYCOM data (1/12° and a daily time step) to that required for model simulations: here, we use its output starting from 1 January 2014 as the earliest date for our simulations. We stress that HYCOM remains a model and its currents do not fully replicate real-world complexity: a possible future investigation would be comparing how simulations using HYCOM data differ with other data sources, including direct measurements based on Lagrangian drifters. For example, in [39], a systematic investigation into the sensitivity of simulated trajectories to the resolution of ocean current data was performed.

5.3. Active movement: navigation

Active movement is parametrized by s and λ, along with those defining the turning distribution. Following marine turtles is understandably difficult and definitive values are speculative, yet logical arguments can provide ranges. We assume individuals have a (unspecified) navigating capacity and periodically reorient towards the island: new active headings are chosen from (3.3) with dominant direction pointing to the island centre from their current location. Note that this assumes individuals *correct* for drift (periodic reassessment of active heading), but do not specifically *compensate* for it: the latter requires detection of the flow direction (see also Discussion).
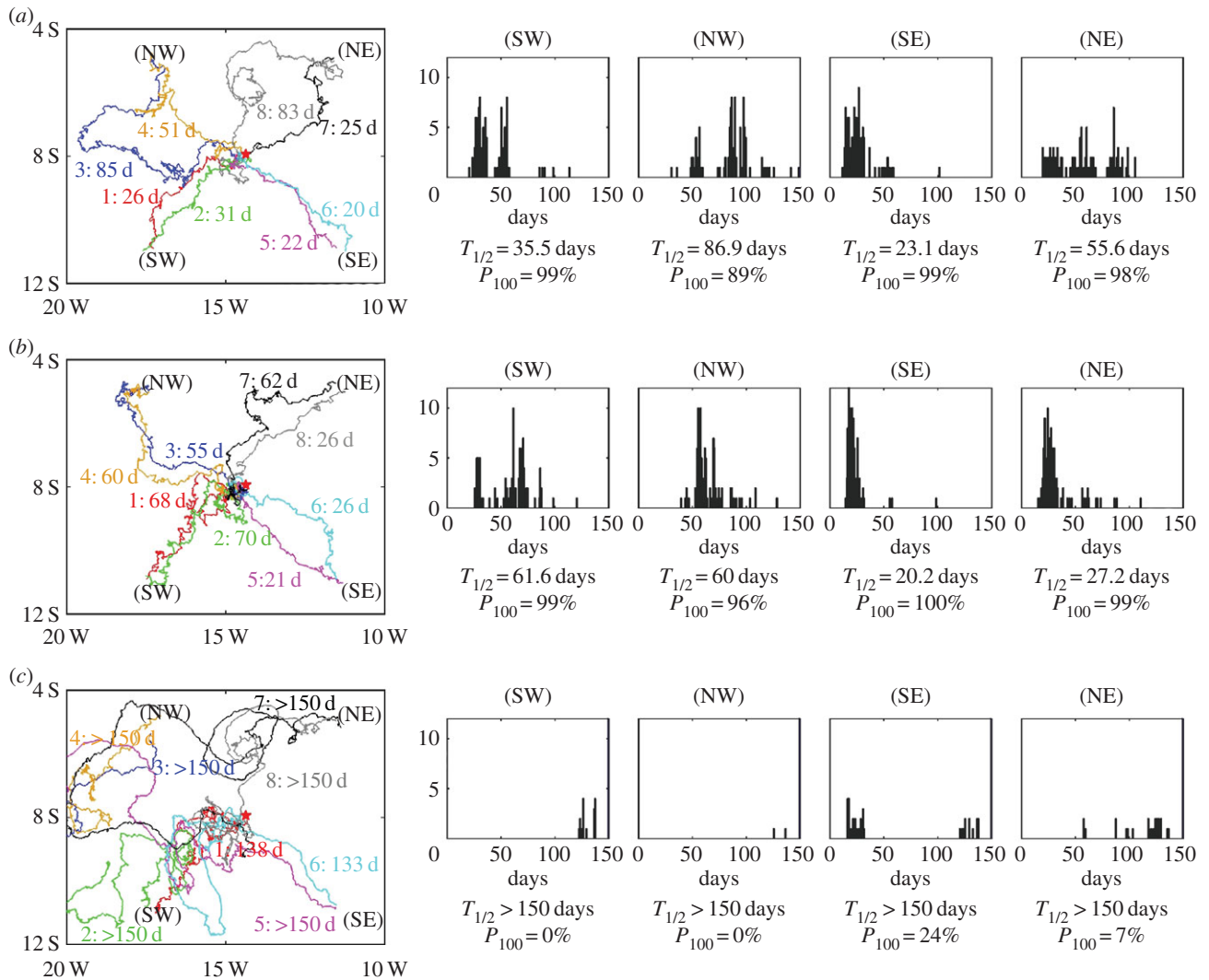
Figure 6. Navigation to AI (red star) in the IBM. Releases at: (*a*) time zero, $s = 50$ km d^{-1}, $k = 1$; (*b*) time $+28$ days, $s = 50$ km d^{-1}, $k = 1$; (*c*) time zero, $s = 30$ km d^{-1}, $k = 1$. In each scenario, we plot: (left) representative tracks of eight individuals, where each track is labelled by an identifier tag and the time of arrival (d = days); (right) population statistics via histograms of the arrival times and population summary data. Simulations time step $\Delta t = 1/8$th hour. (Online version in colour.)

This assumption lies in accordance with conclusions from tracking studies [40,41]. We assume $k \in [0, 3]$ as previously.

We take active speed $s \in [0, 80]$ km d^{-1} [42]: $s = 0$ corresponds to a passive drifter while upper values lie at the energetic limits for sustained swimming. We set $\lambda = 12$ d^{-1} (one turn every 2 h): this would generate an average swim length between turns of up to 5 km. Our rationale is that large-scale navigating cues are unlikely to significantly change over shorter lengths; on the other hand, less frequent assessment would be less than optimal for drift correction. We remark that direct sources for estimating λ could be based on a turtle re-estimating its direction each time it surfaces [43], or through careful analysis of tracking study data: this will be considered in a future, more refined study.

5.4. Individual model simulations

The IBM generates both individual and population data (figure 6). We consider various scenarios in which populations (for each, $N = 100$) are simultaneously released NE, SE, SW and NW from the island. For each row, the leftmost panel shows representative tracks from each release location, while other panels show histograms for island arrival times. We also tabulate two population success statistics:

$T_{1/2}$, the time half the population has arrived at the island; and P_{100}, the percentage that have reached the island 100 days post-release.

For figure 6*a*, we set $s = 50$ km d^{-1}, $k = 1$ and a release at time zero: this represents a stronger swimmer, with the mean swimming speed lying above the average underlying current, although there are times and locations where the latter may be considerably faster (ocean current snapshots can be seen in figure 7). Consequently, paths can be highly circuitous before reaching the island (e.g. tracks 3 and 8), despite consistent reorientation with respect to the island goal. Overall, however, populations are successful in eventually reaching the island.

We observe a broad spectrum of arrival times between the different populations: $T_{1/2}$ ranges from approximately 23 days (for the SE population) to approximately 90 days for the NW population; histograms range from tightly clustered (e.g. SE) to scattered (e.g. NE, NW). We also observe considerable variation within a population: for example, the NE population has arrival times varying from 20 days to more than 100. Differences between the tracks from two individuals at a single release location stem from (smallish) variations in their exact starting location and randomness entering their active movement path, along with the different currents encountered.
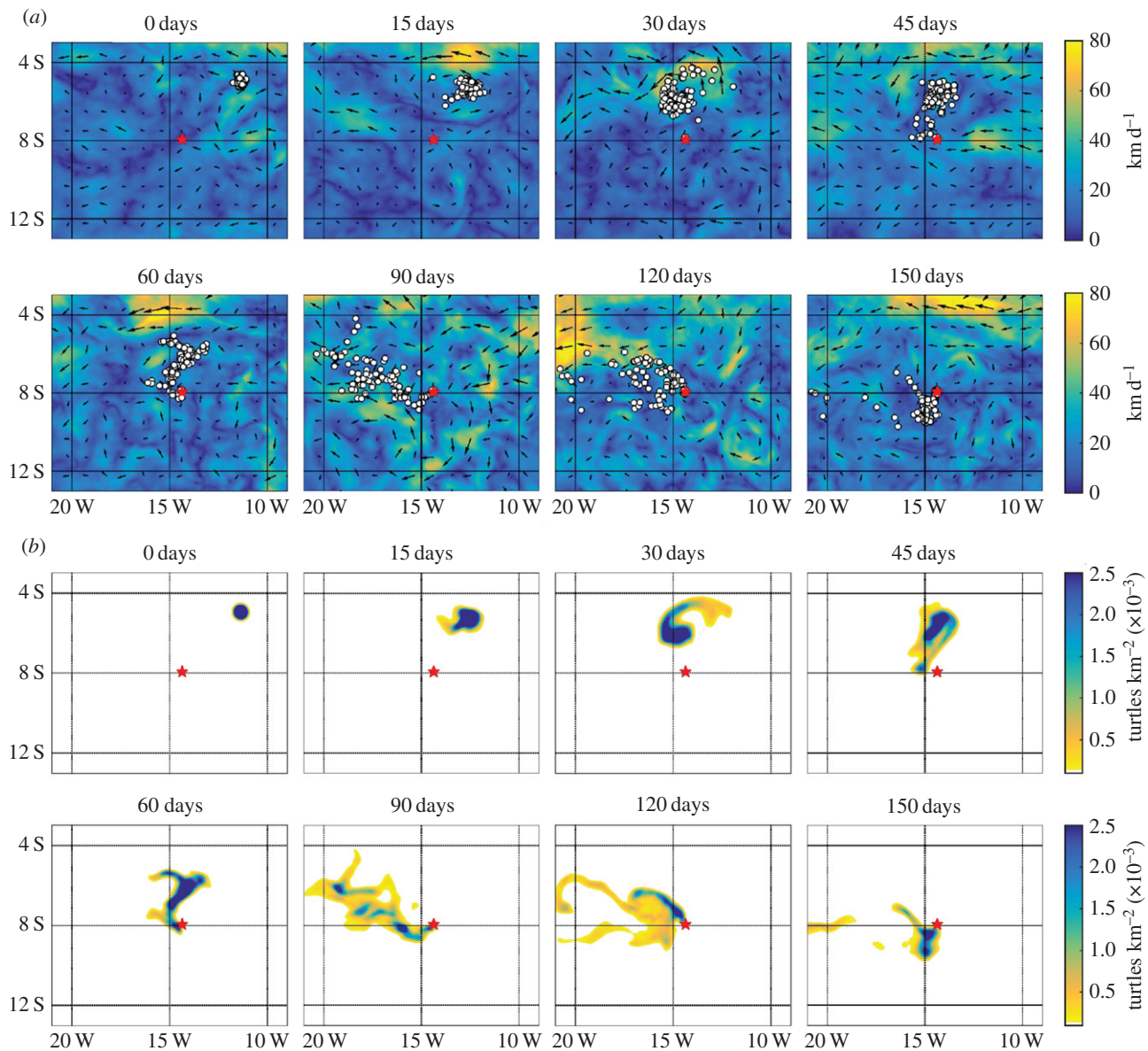
Figure 7. Comparison between the IBM and macroscopic model. (*a*) IBM: 100 individuals are released at time zero at the NE location. In each subplot, we show their positions (white circles) at the indicated times, superimposed on ocean currents. Current data are illustrated by its direction (arrows) and magnitude (arrow length/density map). Here, we consider a slower navigator ($s = 30$ km d^{-1}, $k = 1$); for other parameters, see text. (*b*) Macroscopic model (2.3) under the same initial set-up, parameters and ocean currents. $m(t, \mathbf{x})$ indicated by density map, where the scale indicates the number per square kilometre; white regions represent a density below 10^{-4}. The red star marks AI. (Online version in colour.)

Compared against the fairly consistent tracks produced for constant/uniform flows (e.g. figure 3*a*), the large variations are undoubtedly down to magnification by currents. We highlight trajectories 7 and 8 (both NE) in figure 6*a*: while these turtles have identical release times, active movement parameters and close starting locations, turtle 7 more or less directly homes by the 25th day, whereas turtle 8 becomes enveloped in an eddy before homing on the 83rd day.

This current impact can be further investigated via a later release date (+28 days) (figure 6*b*). Populations remain successful overall yet particular statistics change enormously: NW, NE and SE populations all have an easier island passage yet the SW population is significantly delayed ($T_{1/2}$ is almost doubled). Hence, changes in the currents can be expected to significantly impact on island navigation. Note that the SE population typically appears the most successful, suggesting that releases from this position receive optimal currents.

To test the impact of active movement characteristics, we reduce s: in figure 6*c*, we set $s = 30$ km d^{-1}, $k = 1$ and a release

at time zero. The balance between passive and active movement is shifted from the latter to the former and navigation becomes troublesome: paths are tortuous and only a tiny fraction reach the island (in the timeframe). A similar finding is obtained when reducing k. These findings echo those earlier, that a critical transition in population success occurs according to movement/flow characteristics.

5.5. Individual to macroscopic model

We compare the IBM and continuous model, testing the latter's capacity to predict distributions of the former. Simulations in figure 7 are based on a NE release at time zero, $s = 30$ km d^{-1} and $k = 1$. Figure 7*a* plots the data from the IBM, superimposing simulated turtle positions on the ocean currents at various times following release. In figure 7*b*, we plot $m(t, \mathbf{x})$, obtained by solving equation (2.3) subject to the same currents and (3.4) calculated using the same active movement parameters. A movie of these simulations is available (electronic supplementary material, movie S1).
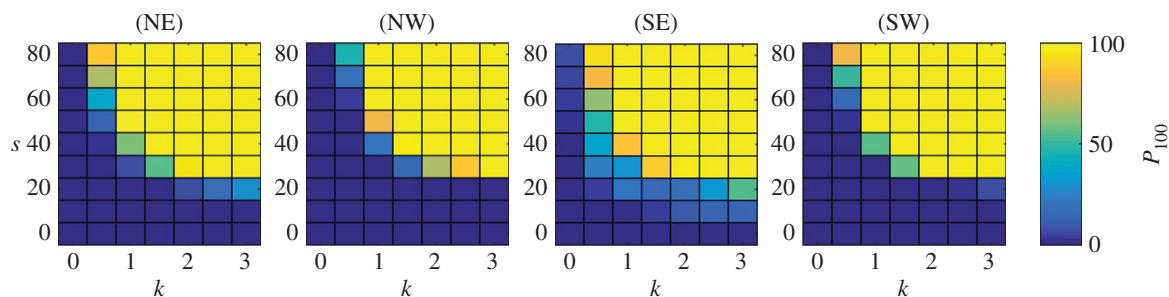
Figure 8. Population summary statistics (P_{100}) over a range of (s, k) parameter combinations. Scales indicated on the right. (Online version in colour.)

The closeness between distributions suggests that the macroscopic model offers an excellent quantitative approximation for population statistics of the IBM: investigations for other scenarios yield a similarly close match, with further examples and movies in the electronic supplementary material, including for a pure drifter and a stronger swimmer. As a point of note, the simulation using (2.3) takes the order of minutes, while that of the IBM takes more than an hour[2]: the latter's inefficiency stemmed from frequent interpolation between an individual's position and drift data, burdensome as the population increases.

We exploit the efficiency of the macroscopic model to investigate population success as s and k are varied across their full ranges (figure 8). The simulations focus on a release date of time zero: broadly, releases at other times generate similar conclusions yet exact statistics change due to the different currents, as noted above. As for the idealized case, we again observe a fairly sharp transition between overall population success and failure. The lines $s = 0$ and $k = 0$ correspond to 'drifter' and 'random mover' populations, respectively. Neither are successful: a tiny fraction are assisted by fortuitous currents, yet the vast majority fail. Navigation is understandably straightforward at the largest values of s and k: populations arrive within very short times (order of a week to two weeks). However, while the upper swimming speeds (approx. $0.9 \, \mathrm{m \, s^{-1}}$) are feasible short term, whether they remain so over days to weeks is less certain. Similarly, upper values of k represent a fairly precise orienteering mechanism, with more than half of the turns falling within less than $\pm 25°$ of the true bearing.

Of course, population success does not require both speeds and turning rates to lie at the upper reaches of these ranges: close to 100% of the populations can arrive at the island inside 100 days for more moderate combination of $k = 1.5$ and $s = 40 \, \mathrm{km \, d^{-1}}$. Further, the nature of the curve between success and failure suggests that a weak navigator can compensate by fast swimming, while a slower mover can compensate via a precise navigation. We should note, however, that 100 days is quite a long time and our model does not allow individuals to 'give up', nor does it consider 'blind spots' in the navigating information: our present study is purposefully simple to concentrate on the essential relationship between navigation and currents.

6. Discussion

The aim has been to describe a common framework for modelling navigation in flowing environments. We achieve this by connecting IBMs to continuous models: the former allows individual-level data to be generated, while the latter offers an efficient path to population statistics. Further, the continuous model can be analysed via the method of characteristics, creating a route back to 'average' individual-level movement. This process formally connects data inputs for the IBM (e.g. ocean currents, tracking studies) to the macroscopic model and will allow formal testing of different hypotheses for navigation, through comparing simulation/analytical predictions with empirical observations: for similar studies, see [44].

We illustrated this for generic movement classes: drifters, random movers and navigators. Formally, drifters are organisms/particles that simply float and are convected by currents: certain studies assume this if active movement is smallish (e.g. [12]), yet it must be considered carefully since even small amounts of oriented swimming can alter overall behaviour [10,11]. A navigator corresponds to an organism that actively swims, periodically assessing its environment and biasing its active direction accordingly. The oriented turning response was incorporated via a von Mises distribution, and the macroscopic model is of drift-anisotropic diffusion form. The von Mises distribution is a standard in the field, although other forms are available and different models may result [27].

For the examples here, the continuous model closely matched the statistics of the IBM. This good agreement, however, cannot be expected a priori: for example, if the problem length and time scales are not sufficiently macroscopic. Interactions between individuals should also be considered, as the formal process assumes these are negligible: this appears reasonable for dispersed marine turtles, yet becomes less certain for, say, fish schooling or bird flocking. Overall, these warnings highlight the advantages of a twin approach: macroscopic models offer analytical convenience, yet may not apply to the full spectrum of situations allowed by the underlying IBM.

To demonstrate the methodology within a concrete problem, we primarily focused on ocean navigation. The framework, however, is general and can be extended to other scenarios, such as flight navigation: indeed, an earlier application of our approach was used in [29] to investigate butterfly hilltopping, albeit for negligible wind. IBM models based on principles similar to those here have been extensively applied to bird and insect navigation (e.g. [13]), and it would be intriguing to adapt our model to accommodate the peculiarities of these applications: for example, by incorporating 'resting phases' in response to unfavourable atmospheric conditions, or flight adaptation towards favourable winds.

Our model has assumed that turtles simply correct for flow by periodically reorienting in the direction of the (island) goal. Whether an organism corrects or can actively compensate (by detecting flow direction) is a significant question [6]: a capacity to determine flow direction has

been suggested for a variety of airborne (moths and songbirds [45]) and aquatic species (jellyfish [9] and juvenile turtles [46]). Our framework can be adapted to investigate such phenomena: for example, the navigational response can be based on both the flow direction and the overall direction of some goal. More generally, our model can be extended to explicitly include a proposed navigating cue(s): for example, the varying geomagnetic field or a transported chemical cue. Chemical cues are certainly well known in the context of pheromone following, and ocean/wind-borne signals have also been proposed as potential guidance cues for marine turtles (e.g. [35,47]).

The homing problem can be understood as a *mean free passage time* (MFPT) problem, used in ecology to estimate the expected time for individuals to reach a target [48]. Recently, Kurella *et al.* [49] considered active navigators with isotropic diffusion and solved the MFPT problem via asymptotic methods for small targets. This acts as a special case of our problem, corresponding to conservative drift and isotropic and constant diffusion. An interesting, yet non-trivial, question emerges on formulating and solving the MFPT problem for non-isotropic active movement within a non-conservative and dynamic flow field, as relevant here.

We quantitatively assessed critical relationships for successful homing: for both idealized and AI scenarios, we obtain a relatively abrupt boundary between population-level failure and success as key characteristic parameters (flow, swim speed, navigating strength) are varied (figures 5 and 8). For populations with characteristic parameters lying firmly inside the 'success region', navigation should be reasonably robust with respect to currents. Populations lying closer to the boundary, however, may show sensitivity to currents and large individual variations. Consequently, we expect the impact of currents on homing to be highly variable from case to case. In the context of AI, simulated turtles do home for relatively moderate swimming speeds and navigating strength but reasonable parameters may lie close to the boundary. We could therefore expect a range between relatively straightforward and convoluted homing when observed individually, echoing the variability in re-homing attempts by displaced turtles (e.g. [50]). Of course, such findings must be viewed cautiously given the simplistic framework here: a key aim is to expand these preliminary findings and address the greater complexities expected in the natural environment.

Endnotes

[1] A precise condition is considerably harder to find: it would further depend on parameters such as starting locations, goal size and simulation timeframe.

[2] Neither method can be regarded as 'optimal' and this is not a formal analysis: our intention is to stress that, generally, macroscopic models are more efficient for population studies.

Appendix A. Method of characteristics

From (3.4), we introduce coefficients:

$$c_1(k) := s\frac{I_1(k)}{I_0(k)}, \quad c_2(k) := \frac{s^2}{2\lambda}\left(1 - \frac{I_2(k)}{I_0(k)}\right)$$

and

$$c_3(k) := \frac{s^2}{\lambda}\left(\frac{I_2(k)}{I_0(k)} - \frac{I_1(k)^2}{I_0(k)^2}\right), \tag{A 1}$$

where $c_1(k)$ describes active drift and increases with k. $c_2(k)$ defines the degree of isotropic diffusion and decreases with k. $c_3(k)$ defines the degree of anisotropy, is negative and is an order of magnitude smaller than c_1 and c_2.

The idealized scenario takes $\mathbf{u}(t, x) = (u_x, 0)$, where $u_x \geq 0$, and active orientation is towards the origin. Consequently, an individual at position (x, y) has active direction $-(x, y)/\sqrt{x^2 + y^2}$ and, from (3.1) and (A 1), we find

$$\mathbf{a}(t, x) = -c_1\begin{pmatrix} x/r \\ y/r \end{pmatrix}, \quad r = \sqrt{x^2 + y^2}$$

and

$$\mathbb{D}(t, x) = c_2\begin{pmatrix} 1 & 0 \\ 0 & 1 \end{pmatrix} + c_3\begin{pmatrix} \frac{x^2}{r^2} & \frac{xy}{r^2} \\ \frac{xy}{r^2} & \frac{y^2}{r^2} \end{pmatrix}.$$

The divergence of $\mathbb{D}$ is

$$\nabla \cdot \mathbb{D} = \partial_i \mathbb{D}^{ij} = \frac{c_3}{r^4}\begin{pmatrix} 2xr^2 - x^2 2x + xr^2 - xy2y \\ yr^2 - xy2x + 2yr^2 - y^2 2y \end{pmatrix} = \frac{c_3}{r^2}\begin{pmatrix} x \\ y \end{pmatrix}.$$

Hence, (2.6) is as given by equations (4.1) of the main text for the ideal flow case.

To investigate the success/failure threshold, we perform a steady-state analysis. The singular nature of (4.1) at (0, 0), however, demands a modification: we multiply the right-hand sides of (4.1) by $x^2 + y^2$ to obtain the following system with identical orbits:

$$\dot{x} = u_x(x^2 + y^2) - c_1 x\sqrt{x^2 + y^2} - c_3 x$$

and

$$\dot{y} = -c_1 y\sqrt{x^2 + y^2} - c_3 y. \tag{A 2}$$

Steady states and their stabilities are as follows.

(1) SS_1 (0,0) is always unstable. Eigenvalues are $\lambda_1 = \lambda_2 = -c_3$ and, since $c_3 < 0$, are positive. Naively one would expect (0,0) to be an attractor, since it defines the active heading. However, c_3 is a coefficient of the variance–covariance matrix and expresses uncertainty in the direction choice. This uncertainty (mathematically) means that the origin is always 'just missed'.

(2) SS_2 $(c_3/(u_x + c_1), 0)$ lies in the negative half-plane, since $c_3 < 0$. SS_2 is always a saddle point, with stability in the x-direction and instability in the y-direction.

(3) SS_3 If $c_1 > u_x$, then there exists a third steady state $(-c_3/(c_1 - u_x), 0)$:

— if $c_1 > u_x$, it exists and forms a local and global attractor, defining the point of convergence for all orbits;
— if $c_1 < u_x$, all non-trivial orbits (except steady states and stable orbits of SS_2) are swept out of the domain.

Summarizing, we conclude:

Lemma A.1. *When $c_1 > u_x$, trajectories converge to SS_3.*

How does this translate to goal-finding? The above reveals that all trajectories eventually hit the goal if SS_3 lies inside it: hence, *given sufficient time and assuming the goal is sufficiently large*, lemma A1 guarantees success and condition (4.2) provides an approximate condition for the required navigational strength k. Of course, we must stress its approximate nature,

yet for the present application it provides a more than reasonable estimate (e.g. figure 5a3). One should also note that failure to satisfy lemma A1 does not necessarily translate to overall failure: a trajectory could still hit the goal during its passage, even if it is eventually swept out of the domain, by virtue of favourable initial conditions.

References

1. Darwin C. 1873 Perception in the lower animals. *Nature* **7**, 360. (doi:10.1038/007360c0)

2. Lohmann KJ, Luschi P, Hays GC. 2008 Goal navigation and island-finding in sea turtles. *J. Exp. Mar. Biol. Ecol.* **356**, 83–95. (doi:10.1016/j.jembe.2007.12.017)

3. Putman NF, Jenkins ES, Michielsens CGJ, Noakes DLG. 2014 Geomagnetic imprinting predicts spatiotemporal variation in homing migration of pink and sockeye salmon. *J. R. Soc. Interface* **11**, 20140542. (doi:10.1098/rsif.2014.0542)

4. Luschi P, Hays GC, Papi F. 2003 A review of long-distance movements by marine turtles, and the possible role of ocean currents. *Oikos* **103**, 293–302. (doi:10.1034/j.1600-0706.2003.12123.x)

5. Gaspar P, Georges JY, Fossette S, Lenoble A, Ferraroli S, Le Maho Y. 2006 Marine animal behaviour: neglecting ocean currents can lead us up the wrong track. *Proc. R. Soc. B* **2730**, 2697–2702. (doi:10.1098/rspb.2006.3623)

6. Chapman JW, Klaassen RHG, Drake VA, Fossette S, Hays GC, Metcalfe JD, Reynolds AM, Reynolds DR, Alerstam T. 2011 Animal orientation strategies for movement in flows. *Curr. Biol.* **21**, R861–R870. (doi:10.1016/j.cub.2011.08.014)

7. Grimm V, Railsback SF. 2005 *Individual-based modeling and ecology.* Princeton, NJ: Princeton University Press.

8. Staaterman E, Paris CB. 2014 Modelling larval fish navigation: the way forward. *ICES J. Mar. Sci.* **71**, 918–924. (doi:10.1093/icesjms/fst103)

9. Fossette S, Gleiss AC, Chalumeau J, Bastian T, Armstrong CD, Vandenabeele S, Karpytchev M, Hays GC. 2015 Current-oriented swimming by jellyfish and its role in bloom maintenance. *Curr. Biol.* **25**, 342–347. (doi:10.1016/j.cub.2014.11.050)

10. Putman NF, Verley P, Shay TJ, Lohmann KJ. 2012 Simulating transoceanic migrations of young loggerhead sea turtles: merging magnetic navigation behavior with an ocean circulation model. *J. Exp. Biol.* **215**, 1863–1870. (doi:10.1242/jeb.067587)

11. Scott R, Marsh R, Hays GC. 2012 A little movement orientated to the geomagnetic field makes a big difference in strong flows. *Mar. Biol.* **159**, 481–488. (doi:10.1007/s00227-011-1825-1)

12. Bonhommeau S, Le Pape O, Gascuel D, Blanke B, Tréguier A-M, Grima N, Vermard Y, Castonguay M, Rivot E. 2009 Estimates of the mortality and the duration of the trans-Atlantic migration of European eel *Anguilla anguilla* leptocephali using a particle

tracking model. *J. Fish Biol.* **74**, 1891–1914. (doi:10.1111/j.1095-8649.2009.02298.x)

13. Shamoun-Baranes J, Leyrer J, van Loon E, Bocher P, Robin F, Meunier F, Piersma T. 2010 Stochastic atmospheric assistance and the use of emergency staging sites by migrants. *Proc. R. Soc. B* **277**, 1505–1511. (doi:10.1098/rspb.2009.2112)

14. Chapman JW, Nesbit RL, Burgin LE, Reynolds DR, Smith AD, Middleton DR, Hill JK. 2010 Flight orientation behaviors promote optimal migration trajectories in high-flying insects. *Science* **327**, 682–685. (doi:10.1126/science.1182990)

15. Willis J. 2011 Modelling swimming aquatic animals in hydrodynamic models. *Ecol. Mod.* **222**, 3869–3887. (doi:10.1016/j.ecolmodel.2011.10.004)

16. Shamoun-Baranes J, Bouten W, van Loon E. 2010 Integrating meteorology into research on migration. *Int. Comp. Biol.* **50**, 280–292. (doi:10.1093/icb/icq011)

17. Sibert JR, Hampton J, Fournier DA, Bills PJ. 1999 An advection–diffusion–reaction model for the estimation of fish movement parameters from tagging data, with application to skipjack tuna (*Katsuwonus pelamis*). *Can. J. Fish. Aquat. Sci.* **56**, 925–938.

18. Pachepsky E, Lutscher F, Nisbet RM, Lewis MA. 2005 Persistence, spread and the drift paradox. *Theor. Pop. Biol.* **67**, 61–73. (doi:10.1016/j.tpb.2004.09.001)

19. Tyson R, Thistlewood H, Judd GJR. 2007 Modelling dispersal of sterile male codling moths, *Cydia pomonella*, across orchard boundaries. *Ecol. Model.* **205**, 1–12. (doi:10.1016/j.ecolmodel.2006.12.038)

20. Codling EA, Plank MJ, Benhamou S. 2008 Random walk models in biology. *J. R. Soc. Interface* **5**, 813–834. (doi:10.1098/rsif.2008.0014)

21. Hillen T, Painter KJ. 2013 Transport and anisotropic diffusion models for movement in oriented habitats. In *Dispersal, individual movement and spatial ecology: a mathematical perspective.* Berlin, Germany: Springer.

22. Faugeras B, Maury O. 2007 Modeling fish population movements: from an individual-based representation to an advection–diffusion equation. *J. Theor. Biol.* **247**, 837–848. (doi:10.1016/j.jtbi.2007.04.012)

23. Gómez-Mourelo P. 2005 From individual-based models to partial differential equations: an application to the upstream movement of elvers. *Ecol. Model.* **188**, 93–111. (doi:10.1016/j.ecolmodel.2005.05.014)

24. Othmer HG, Dunbar SR, Alt W. 1988 Models of dispersal in biological systems. *J. Math. Biol.* **26**, 263–298. (doi:10.1007/BF00277392)

25. Hays GC, Åkesson S, Broderick AC, Glen F, Godley BJ, Luschi P, Martin C, Metcalfe JD, Papi F. 2001 The diving behaviour of green turtles undertaking oceanic migration to and from Ascension Island: dive durations, dive profiles and depth distribution. *J. Exp. Biol.* **204**, 4093–4098.

26. Batschelet E. 1981 *Circular statistics in biology.* London, UK: Academic Press.

27. Codling EA, Bearon RN, Thorn GJ. 2010 Diffusion about the mean drift location in a biased random walk. *Ecology* **91**, 3106–3113. (doi:10.1890/09-1729.1)

28. McKenzie HW, Merrill EH, Spiteri RJ, Lewis MA. 2012 How linear features alter predator movement and the functional response. *Interface Focus* **2**, 205–216. (doi:10.1098/rsfs.2011.0086)

29. Painter KJ. 2014 Multiscale models for movement in oriented environments and their application to hilltopping in butterflies. *Theor. Ecol.* **7**, 53–75. (doi:10.1007/s12080-013-0198-0)

30. Lohmann KJ, Lohmann CMF, Ehrhart LM, Bagley DA, Swing T. 2004 Geomagnetic map used in sea-turtle navigation. *Nature* **428**, 909–910. (doi:10.1038/428909a)

31. Lohmann KJ, Cain SD, Dodge SA, Lohmann CMF. 2001 Regional magnetic fields as navigational markers for sea turtles. *Science* **294**, 364–366. (doi:10.1126/science.1064557)

32. Lohmann KJ, Putman NF, Lohmann CMF. 2012 The magnetic map of hatchling loggerhead sea turtles. *Curr. Opin. Neurobiol.* **22**, 336–342. (doi:10.1016/j.conb.2011.11.005)

33. Mortimer JA, Carr A. 1987 Reproduction and migrations of the Ascension Island green turtle (*Chelonia mydas*). *Copeia* **1987**, 103–113. (doi:10.2307/1446043)

34. Godley BJ, Broderick AC, Hays GC. 2001 Nesting of green turtles (*Chelonia mydas*) at Ascension Island, South Atlantic. *Biol. Conserv.* **97**, 151–158. (doi:10.1016/S0006-3207(00)00107-5)

35. Koch AL, Carr A, Ehrenfeld DW. 1969 The problem of open-sea navigation: the migration of the green turtle to Ascension Island. *J. Theor. Biol.* **22**, 163–179. (doi:10.1016/0022-5193(69)90085-X)

36. Lohmann KJ, Lohmann CM. 1996 Detection of magnetic field intensity by sea turtles. *Nature* **380**, 59–61. (doi:10.1038/380059a0)

37. Luschi P. 2013 Long-distance animal migrations in the oceanic environment: orientation and navigation correlates. *ISRN Zool.* **2013** 1–23. (doi:10.1155/2013/631839)

38. Bleck R. 2002 An oceanic general circulation model framed in hybrid Isopycnic–Cartesian coordinates. *Ocean Mod*. **4**, 55–88. (doi:10.1016/S1463-5003(01) 00012-9)

39. Putman NF, He R. 2013 Tracking the long-distance dispersal of marine organisms: sensitivity to ocean model resolution. *J. R. Soc. Interface* **10**, 20120979. (doi:10.1098/rsif.2012.0979)

40. Girard C, Sudre J, Benhamou S, Roos D, Luschi P. 2006 Homing in green turtles *Chelonia mydas*: oceanic currents act as a constraint rather than as an information source. *Mar. Ecol. Prog. Ser*. **322**, 281–289. (doi:10.3354/meps322281)

41. Luschi P, Benhamou S, Girard C, Ciccione S, Roos D, Sudre J, Benvenuti S. 2007 Marine turtles use geomagnetic cues during open-sea homing. *Curr. Biol*. **17**, 126–133. (doi:10.1016/j.cub.2006.11.062)

42. Wyneken J. 1997 *The biology of sea turtles*, pp. 165–198. Boca Raton, FL: CRC Press.

43. Narazaki T, Sato K, Abernathy KJ, Marshall GJ, Miyazaki N. 2009 Sea turtles compensate deflection of heading at the sea surface during directional travel. *J. Exp. Biol*. **212**, 4019–4026. (doi:10.1242/jeb.034637)

44. Hays GC, Christensen A, Fossette S, Schofield G, Talbot J, Mariani P. 2014 Route optimisation and solving Zermelo's navigation problem during long distance migration in cross flows. *Ecol. Lett*. **17**, 137–143. (doi:10.1111/ele.12219)

45. Chapman JW, Nilsson C, Lim KS, Bäckman J, Reynolds DR, Alerstam T, Reynolds AM. 2015 Detection of flow direction in high-flying insect and songbird migrants. *Curr. Biol*. **25**, R751–R752. (doi:10.1016/j.cub.2015.07.074)

46. Kobayashi DR, Farman R, Polovina JJ, Parker DM, Rice M, Balazs GH. 2014 'Going with the flow' or not: evidence of positive rheotaxis in oceanic juvenile loggerhead turtles (*Caretta caretta*) in the south pacific ocean using satellite tags and ocean circulation data. *PLoS ONE* **9**, e103701. (doi:10.1371/journal.pone.0103701)

47. Endres CS, Lohmann KJ. 2013 Detection of coastal mud odors by loggerhead sea turtles: a possible mechanism for sensing nearby land. *Mar. Biol*. **160**, 2951–2956. (doi:10.1007/s00227-013-2285-6)

48. Redner S. 2001 *A guide to first-passage processes*. Cambridge, UK: Cambridge University Press.

49. Kurella V, Tzou JC, Coombs D, Ward MJ. 2015 Asymptotic analysis of first passage time problems. *Bull. Math. Biol*. **77**, 83–125. (doi:10.1007/s11538-014-0053-5)

50. Åkesson S, Broderick AC, Glen F, Godley BJ, Luschi P, Papi F, Hays GC. 2003 Navigation by green turtles: which strategy do displaced adults use to find Ascension Island? *Oikos* **103**, 363–372. (doi:10.1034/j.1600-0706.2003.12207.x)